ACI MATERIALS JOURNAL TECHNICAL PAPER

Title no. 108-M60

Evaluating Surface-Breaking Cracks in Concrete Using Air-Coupled Sensors

by Seong-Hoon Kee, Eulalio Fernández-Gómez, and Jinying Zhu

The purpose of this research is to develop a rapid in-place nondestructive test (NDT) method to evaluate surface-breaking cracks in in-place concrete structures. Air-coupled sensors are used to measure surface wave transmission across surface-breaking cracks in concrete. The surface wave transmission (SWT) method is developed to determine crack depth and characterize cracking damage in concrete structures. In this study, the developed SWT method is used to identify and characterize cracks in three prestressed concrete beams with different degrees of deterioration caused by alkali-silica reaction (ASR) and delayed ettringite formation (DEF). The SWT measurement results are presented as transmission maps and compared with crack patterns and the severity of deterioration. The crack depths determined from the SWT test show good agreement with direct measurements from core samples. The findings demonstrate the potential of the air-coupled SWT method for the in-place evaluation of cracking damage in large concrete structures.

Keywords: air-coupled sensors; nondestructive test; surface-breaking cracks; surface wave transmission.

INTRODUCTION

The deterioration of reinforced concrete structures is generally manifested as surface-breaking cracks in concrete. Characterizing surface-breaking cracks will provide useful information to evaluate the current health condition and future life expectancy of concrete structures and help infrastructure agencies make appropriate rehabilitation decisions. Infrastructure management agencies generally require planned field inspection, which primarily relies on visual examinations and some destructive tests (for example, core extractions); however, a visual examination can only provide superficial information and the results depend on the experience of the inspectors. Destructive tests such as core extraction may provide detailed information about concrete, but they are labor-intensive and time-consuming and cannot cover the entire structure. Therefore, it is important to develop rapid and reliable nondestructive test (NDT) methods for evaluating surface-breaking cracks in in-place, large concrete structures.

Although crack width and density can be directly measured on the concrete surface, crack depth measurement in concrete has always been a challenging task. For crack depth measurement, the time-of-flight diffraction (TOFD) method is the most commonly used NDT method[1-3]; however, the accuracy of the TOFD results is affected by the infiltration of dust and/or water in the cracks and the shape of crack tips. The TOFD method may not always provide reasonable crack depth estimation in field applications.[4,5]

The surface wave transmission (SWT) method has been found to be sensitive to the existence of surface-breaking cracks.[6,7] The SWT method is based on measurements of surface wave transmissions across a surface-breaking crack. In the SWT method, two sensors are located on either side of the crack according to the self-calibrating (SC) procedure[7-9] (refer to Fig. 1). The SC procedure is effective in reducing the experimental variability caused by inconsistent source input and receiver coupling. The transmission coefficient of surface waves is defined as the spectral amplitude ratio between the transmitted surface waves R_{tr} and the incident surface waves R_i in the frequency domain. The depth of a surface-breaking crack can be estimated from the pre-established relation between the transmission coefficient and crack depth (details are described in the background section of this paper). The original SC procedure is a local NDT method that is useful for one crack only. In this study, the authors extend the SWT method to cover wide test areas using the proposed modified SC (MSC) procedure. In addition, using noncontact air-coupled sensors enables consistent measurements and significantly improves test speed. Therefore, the air-coupled SWT method with the MSC technique shows the potential for rapid NDT scanning of in-place concrete structures, especially for large civil infrastructure systems.

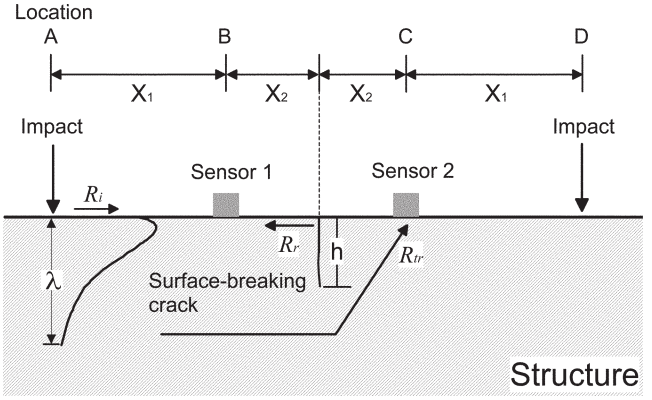

Fig. 1—Surface wave transmission test setup for SC procedure.

The objective of this study is to apply the air-coupled SWT method to identify critical cracks and estimate the depth of surface-breaking cracks in the dapped-end regions of three prestressed concrete trapezoidal box beams. Surface wave transmission was measured on the surfaces of the beams, which experienced different degrees of deterioration caused by alkali-silica reaction (ASR) and delayed ettringite formation (DEF). Noncontact air-coupled sensors were used to improve the signal consistency and test speed for the inspection of large concrete structures. For these purposes,

ACI Materials Journal, V. 108, No. 5, September-October 2011.
MS No. M-2010-296.R2 received October 11, 2010, and reviewed under Institute publication policies. Pertinent discussion including author's closure, if any, will be published in the July-August 2012 *ACI Materials Journal* if the discussion is received by April 1, 2012.

ACI member **Seong-Hoon Kee** *is a Postdoctoral Research Associate at the Center for Advanced Infrastructure and Transportation (CAIT), Rutgers, The State University of New Jersey, New Brunswick, NJ. He received his PhD in civil engineering from the University of Texas at Austin, Austin, TX. He received the 2011 ACI-James Instruments Student Award for Research on NDT of Concrete. His research interests include automated nondestructive testing, structural health monitoring, and the deterioration process of concrete.*

ACI member **Eulalio Fernández-Gómez** *is a PhD Candidate at the University of Texas at Austin. He received his BS in civil engineering from the Universidad Autónoma de Chihuahua, Chihuahua, Mexico, and his MS in structural engineering from the University of Texas at Austin.*

ACI member **Jinying Zhu** *is an Assistant Professor in the Department of Civil, Architectural and Environmental Engineering at the University of Texas at Austin. She received her PhD in civil engineering from the University of Illinois at Urbana-Champaign, Urbana, IL. She is a member of ACI Committees 123, Research and Current Developments; 228, Nondestructive Testing of Concrete; and 231, Properties of Concrete at Early Ages. Her research interests include nondestructive testing of concrete and material characterization using ultrasonic waves.*

the research described herein consists of three parts: 1) a summary of the background for the SWT method; 2) field application of the air-coupled SWT method to in-place concrete structures to identify critical cracks; and 3) the evaluation of the depth of critical cracks using the air-coupled SWT method and verification through comparison with core samples.

RESEARCH SIGNIFICANCE

This study is the first attempt to apply the air-coupled SWT method to the evaluation of surface-breaking cracks in in-place concrete structures. The SWT method is sensitive to the presence and depth variation of surface-breaking cracks in concrete. In addition, the noncontact nature of the air-coupled sensing technique enables rapid acoustic scanning of large concrete structures, which significantly improves the test speed of the method compared to other NDT methods using contact sensors.

BACKGROUND

In this section, the backgrounds of the SWT method are summarized to help readers understand the fundamental basis of the method. Based on the literature reviews, a simplified procedure is proposed to apply the SWT method to in-place concrete structures.

Properties of surface waves

A surface wave is a type of stress wave that propagates along the surface of a solid. The amplitude of surface waves exponentially decays with the distance from the free surface boundary. The surface wave penetration depth depends on frequency: lower-frequency components have deeper penetration depth. When incident surface waves R_i propagate across a surface-breaking crack (refer to Fig. 1), the low-frequency components of the incident surface waves will transmit to the forward scattering field with attenuation (R_{tr}), whereas the high-frequency components will be reflected back (R_r). Consequently, the transmission coefficient of surface waves across a surface-breaking crack, which is defined as the ratio between the spectral amplitudes of R_{tr} and R_i, is strongly dependent on frequency (or wavelength) and the crack depth.

Transmission function

Many studies have shown that the surface wave transmission across a surface-breaking crack is related to the crack depth and wavelength.[10-14] Angel and Achenbach,[10] Achenbach et al.,[15] and Mendelsohn et al.[16] obtained the analytic solution of the scattering field of surface waves caused by a surface-breaking crack. Yew et al.[14] verified the transmission function given by previous researchers[10,15,16] through experimental measurements from aluminum specimens. Cheng and Achenbach[17] also demonstrated that transmission coefficients measured in the far field of a crack ($x_2 \sim 5\lambda$, where x_2 is the distance of a sensor from the crack mouth [refer to Fig. 1]) converge to the analytic solution given in previous studies[10,15,16]. For concrete, a heterogeneous material, the SWT method has proven to be sensitive to the depth of surface-breaking cracks.[6-8,18,19] Hevin et al.[6] obtained the transmission coefficient of a surface wave in the frequency domain using the boundary element method (BEM) and calculated average transmission functions from many different sensor locations. Song et al.[8] obtained the transmission coefficient and normalized crack depth (Tr and h/λ) relation based on numerical simulations (BEM) and experimental studies in the laboratory. Recently, the authors[18] obtained transmission functions through numerical simulations (finite element method [FEM]) and experimental studies in the laboratory. In that study, air-coupled sensors were used to improve test speed and accuracy in transmission measurements.

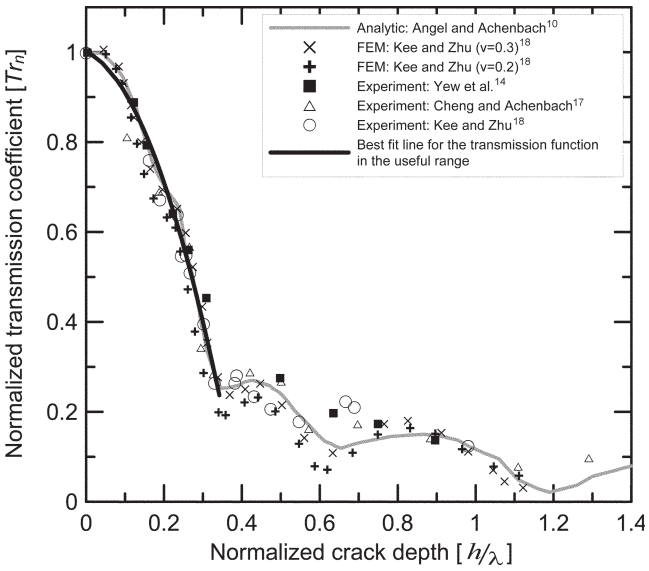

Fig. 2—Surface wave transmission coefficients in approximate far field, based on previous studies.

Previous researchers[18,20-23] noticed that near-field scattering effects (signal enhancement and oscillation in transmission coefficients) significantly affect transmission measurements when sensors are located too close to the crack (that is, $x_2/\lambda < 0.5$ [Reference 23]). The signal enhancement is mainly due to the interference of bulk waves (that is, mode-converted P- and S-waves in front of a surface-breaking crack and bulk waves generated from a tip of a crack) and the direct contribution of incident surface waves.

On the other hand, Fig. 2 shows that transmission functions based on the approximate far-field measurements (that is, $x_2/\lambda > 1.5$ [Reference 23]) tend to converge to the analytic solution.[10,15,16] Yew et al.[14] suggested that the location of sensors should be comparable to or larger than the crack depth to minimize the near-field effect. Cheng and Achenbach[17] observed that Tr converged to the far-field analytic solution when sensors were located 5λ from the

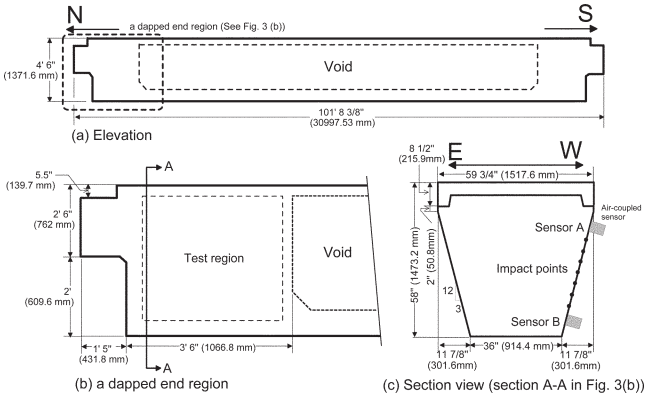

Fig. 3—Typical geometry of prestressed concrete trapezoidal box beam: (a) elevation; (b) side view of dapped-end region; and (c) sectional view of test region and locations of air-coupled sensors and impact forces.

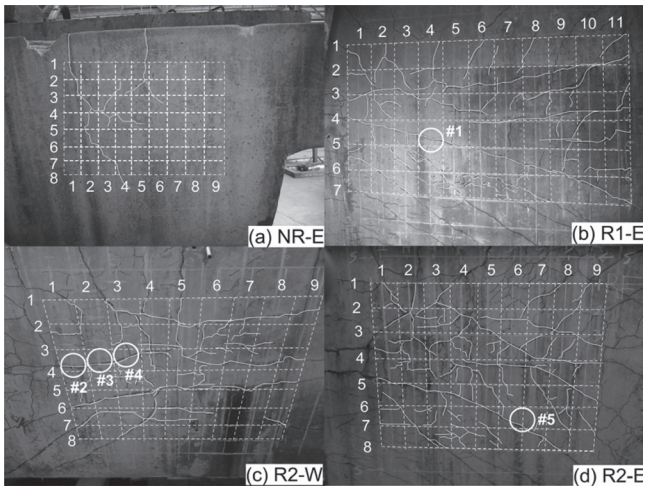

Fig. 4—Crack patterns in test regions of beams.

crack opening. The authors[18] also proposed an approximate near-field size a_n for concrete as follows

$$a_n / \lambda = 1.8h / \lambda + 0.1, \qquad h / \lambda \in [0, 1/3] \tag{1}$$

and demonstrated that the analytic solution is valid for determining the crack depth in concrete if measurements are taken in the approximate far field.

SC procedure

The surface wave transmission coefficient across a surface-breaking crack can be measured by using the SC procedure (refer to the setup in Fig. 1). Previous researchers[7-9] have demonstrated that the SC procedure is effective in reducing the experimental variability caused by inconsistent source input and sensor coupling in surface wave measurements. The surface wave transmission ratios were measured from two opposite directions and processed in the frequency domain. The transmission ratio between locations B and C (refer to Fig. 1) is defined as

$$\left|Tr_{BC}(f)\right| = \left|\sqrt{\frac{S_{AC}S_{DB}}{S_{AB}S_{DC}}}\right| \tag{2}$$

where Tr_{BC} is the transmission coefficient of surface waves propagating across the wave path BC; and S_{ij} is the Fourier transform of the time-domain signal generated by an impact source located at i and measured by a sensor located at j. Further, Tr_{BC} is normalized by $Tr_{BC,0}$ from a crack-free region to eliminate effects caused by geometric attenuation and material damping as follows

$$Tr_n = Tr_{BC} / Tr_{BC,0} \tag{3}$$

SWT analysis based on center frequency

A simplified procedure of the SWT method for field application was proposed by the authors.[18] To obtain accurate crack-depth estimation, the input frequency range of an impact force is carefully selected so that the value of h/λ is within [0, 1/3], in which the transmission is sensitive to crack-depth changes. Once the transmission coefficient is determined, the normalized crack depth h/λ_c corresponding to the center frequency can be found from the pre-established calibration curve. For practical applications, the transmission function of surface waves is expressed in terms of the normalized crack depth h/λ_c using polynomial regression in the useful h/λ ranges (refer to Fig. 2) as follows

$$Tr_n(f_c) = -5.5(h/\lambda_c)^2 - 0.35(h/\lambda_c) + 1 \qquad h/\lambda \in [0,\ 1/3] \tag{4}$$

where $Tr_n(f_c)$ is the normalized transmission coefficient measured at the center frequency f_c; and λ_c is the wavelength of the surface waves at f_c.

It should be noted that the transmission function in Eq. (4) is only valid on the following assumptions:

1. There is only a single surface-breaking crack normal to the free surface of a solid;
2. The incident surface waves are normal to the crack;
3. The wavelengths of the surface waves are sufficiently smaller than the thickness of the solid (that is, $H/2\lambda > 1$, where H is the thickness of the structures); and
4. The transmission coefficients are measured in the far field of a crack.

The simplified SWT method should be carefully applied to in-place concrete structures. Particularly, unevenly distributed cracks with a higher density may increase near-field effects[21,22] and interaction of surface waves between multiple surface-breaking cracks.[24] The validity of the simplified SWT method for in-place concrete structures will be discussed in more detail in the following sections.

FIELD APPLICATION OF AIR-COUPLED SWT METHOD

Test specimens

The SWT method was applied to identify and characterize surface-breaking cracks in the dapped-end regions of three prestressed concrete trapezoidal box beams. The typical geometry of the concrete beams is shown in Fig. 3. The beams have experienced ASR/DEF damage and shown various distributed surface-breaking cracks, especially around the dapped-end regions (refer to Fig. 4). The dapped-end regions of the beam have a solid end block that extends 1050 mm (41.33 in.) past the reentrant corner. Specific descriptions of the beams (for example, reinforcement details, geometry, and mixing properties in fabrication) are given in Reference 25.

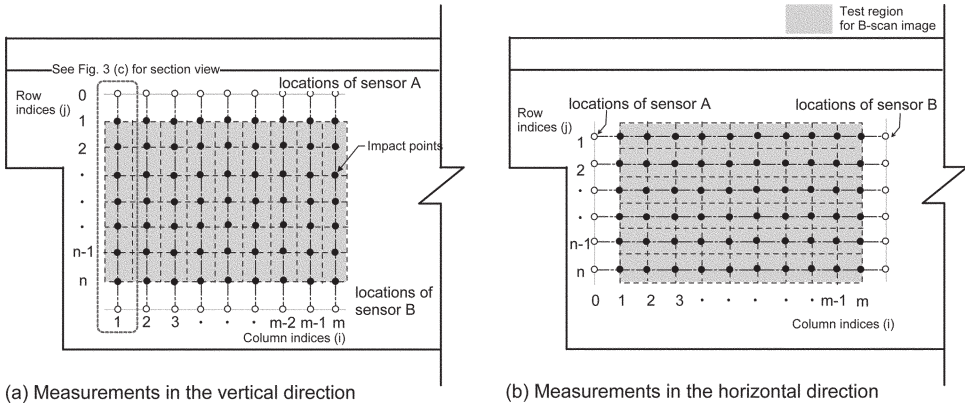

(a) Measurements in the vertical direction

(b) Measurements in the horizontal direction

Fig. 5—Test scheme for transmission maps of test regions based on MSC procedure: (a) scan in vertical direction; and (b) scan in horizontal direction. Impact locations shown as solid dots.

A visual inspection of three beams revealed that the test regions in this study show different degrees of deterioration (crack patterns and crack width). Figure 4 shows four dapped-end sections from three beams. Specimen NR-E, classified as mild damage, had no obvious evidence of deterioration except for several hairline cracks initiating from the top of the beam. In contrast, Specimens R1-E, R2-E, and R2-W, classified as moderately damaged beams, showed extensive typical ASR/DEF cracking. The specimens contained map-like hairline cracks and diagonal cracks with widths ranging from hairline to 1.5 mm (0.06 in.) in the dapped-end regions. The map cracking was dominant near the corner, where heavy reinforcement restrained expansions in the horizontal and vertical directions. In contrast, orient-preferred cracks appear parallel to the compressive stress trajectories for the prestressed beams. The cracks initiated from the top or bottom and continued in a diagonal manner toward the middepth, where the cracks turned horizontal.

Test setup, data acquisition system, and signal processing

Two air-coupled sensors were used to acquire leaky surface wave signals, as shown in Fig. 3(c). The details of the air-coupled sensing technique are described in other publications.[18,26-29] The test setup and data acquisition system for measurements of surface wave transmission were based on the previous research by the authors.[18] A steel ball with a diameter of 14 mm (0.55 in.) was used as an impact source. It generates incident surface waves with a center frequency of approximately 17 kHz. The acquired signals were digitized at a sampling frequency of 10 MHz using an oscilloscope.

MSC procedure

The MSC procedure was used to test large test regions in the concrete beams. Figure 5(a) shows the test scheme to construct a one-dimensional (1-D) transmission map based on a transmission measurement in the vertical direction. The test regions were meshed by grid lines with m columns and n rows, as shown in Fig. 5. For each column, two sensors (Sensors A and B) are located at the ends of test regions (open circles), and an impact force is applied on the grid points 1~n between two sensors. For example, Fig. 3(c) shows the location of Sensors A and B and impact sources of the test region for Column $i = 1$. For an impact source at Row $j = 1$, the Fourier transform of signals received by Sensors A and B are denoted as $\mathbf{S}^1_{(A,1)}$ and $\mathbf{S}^1_{(B,1)}$, respectively. Subsequently, a set of signal data is obtained by moving impact sources from Row $j = 2$ to n. Similarly, by moving Sensors A and B, signals for other columns ($i = 2$~m) are recorded. Finally, transmission coefficients of the test regions defined by two impact sources located at Rows l and k and Column i can be calculated as

$$Tr^i_{lk} = \sqrt{\frac{\mathbf{S}^i_{(A,l)}\mathbf{S}^i_{(B,k)}}{\mathbf{S}^i_{(A,k)}\mathbf{S}^i_{(B,l)}}} \tag{5}$$

where $\mathbf{S}^i_{(A,l)}$ is the Fourier transform of the wave signal generated by an impact source at Row l and measured by Sensor A in a test along Column i. A Hanning window was applied to the time-domain signals to extract the surface wave components[7,8,18] before conducting spectral analysis. Note that Eq. (5) is equivalent to the transmission definition in the SC procedure,[7,9] according to the source-receiver reciprocity.[30]

On the other hand, transmission coefficients measured in the horizontal direction can be obtained in a similar manner. As shown in Fig. 5(b), the transmission coefficient of the test region defined by two impact sources located at Columns l and k and Row i can be calculated as

$$Tr^{lk}_i = \sqrt{\frac{\mathbf{S}^{(A,l)}_i\mathbf{S}^{(B,k)}_i}{\mathbf{S}^{(A,k)}_i\mathbf{S}^{(B,l)}_i}} \tag{6}$$

where $\mathbf{S}^{(A,l)}_i$ is the Fourier transform of the wave signal generated by an impact source at Column l and measured by Sensor A in a test along Row i.

In this study, five repeated signal data sets were collected at the same test location to improve signal consistency. The signal coherence function was used to evaluate the repeatability of the obtained signals. The signal coherence of the signals measured by Sensors A and B is given by

$$SC_{AB}(f) = \frac{\left|\sum_{m=1}^{5} G_{AB}(f)\right|^2}{\sum_{m=1}^{5} G_{AA}(f) \times \sum_{m=1}^{5} G_{BB}(f)} \tag{7}$$

where m is the index of five repeated signal data; and $G_{AB}(f)$, $G_{AA}(f)$, and $G_{BB}(f)$ are the cross spectrum and auto-spectrum

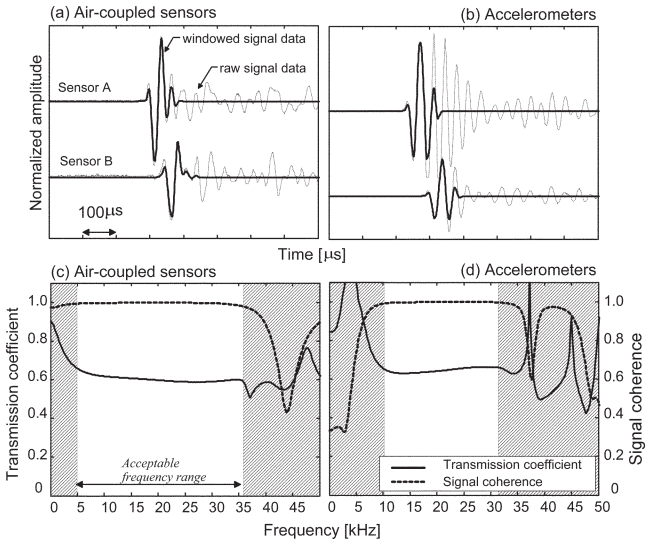

Fig. 6—Comparison of typical signals measured using air-coupled sensors and accelerometers: (a) and (b) show time-domain signals measured using air-coupled sensors and accelerometers, respectively; and (c) and (d) show surface wave transmission coefficient and signal coherence in frequency domain of signals shown in (a) and (b), respectively. Note that time-domain signals in (a) and (b) were normalized by maximum amplitude in incident surface waves measured by Sensor 1.

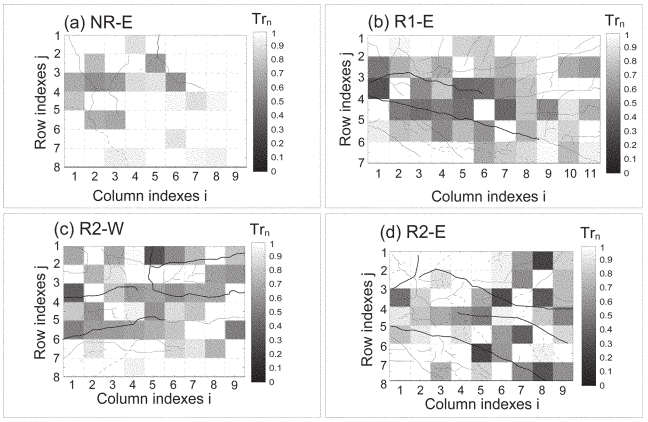

Fig. 7—One-dimensional transmission maps representing transmission coefficients measured in vertical direction from test regions: (a) NR-E; (b) R1-E; (c) R2-W; and (d) R2-E. Both row spacing (distance between impact points) and column spacing (horizontal sensor shift) are 10 cm (3.94 in.).

functions between two time-domain signals measured by Sensors A and B, which are $\mathbf{V}^{i}_{(A,l)}$ and $\mathbf{V}^{i}_{(B,l)}$ for the vertical measurements or $\mathbf{V}_{i}^{(A,l)}$ and $\mathbf{V}_{i}^{(B,l)}$ for the horizontal measurements. Similarly, for an impact at Row k, $SC_{BA}(f)$ can also be calculated from two time-domain signals $\mathbf{V}^{i}_{(A,k)}$ and $\mathbf{V}^{i}_{(B,k)}$ (or $\mathbf{V}_{i}^{(A,k)}$ and $\mathbf{V}_{i}^{(B,k)}$). The averaged $SC(f)$ is defined as

$$SC(f) = \sqrt{SC_{AB}(f)SC_{BA}(f)} \tag{8}$$

which ranges from 0 to 1.0. A value close to 1.0 indicates good signal quality and repeatability. Finally, five transmission functions were then arithmetically averaged in the frequency domain. In addition, the measured surface wave transmission coefficients were further normalized by transmission coefficients measured from a solid region without cracks. This procedure will eliminate the geometric spreading effects caused by a point source and material damping.

Air-coupled sensors versus accelerometers

Accelerometers directly measure the surface wave response on the test surface, whereas air-coupled sensors measure air-pressure disturbance caused by leaky surface waves propagating on the surface. When the air-coupled sensors are placed very close to the surface, the pressure responses are proportional to the surface responses. Figure 6 shows the comparison between air-coupled sensors and accelerometer measurements. Figure 6(a) shows typical time-domain signals measured by two air-coupled sensors in a crack-free region on the concrete specimen with mild damage (Specimen NR-W). The raw signal data and windowed signal data are presented as dash lines and solid lines, respectively. For comparison purposes, the time-domain signal data measured by accelerometers at the same location are also shown in Fig. 6(b). A strong adhesive was used to ensure a good contact condition between the sensors and the concrete surface.

Figure 6(c) and (d) is the transmission coefficients and signal coherence functions of the windowed time-domain signals shown in Fig. 6(a) and (b), respectively. Both the air-coupled sensors and accelerometers give good signal coherence (greater than 0.98) in the frequency range of 10 to 30 kHz. In this frequency range, measurements from the air-coupled sensors and the accelerometers show good agreements, especially around the center frequency (~17 kHz). This result shows that air-coupled sensors provide the same accuracy as accelerometers in the frequency range used in this study.

EVALUATION OF SURFACE-BREAKING CRACKS USING AIR-COUPLED SWT METHOD

Identification of critical cracks using image technique

Figure 7(a) through (d) shows 1-D transmission maps representing transmission coefficients measured from test regions in Specimens NR-E, R1-E, R2-E, and R2-W, respectively. The size of the transmission maps was adjusted according to the size of the end block region of the beams. The spatial resolution of the transmission maps was determined so that the grid size is comparable to the wavelength of incident surface waves, which was 10 cm (3.94 in.) in this study. Each pixel of the maps presents the normalized transmission coefficients of surface waves at the center frequencies. Transmission coefficients corresponding to 1 and 0 are presented in white and black. Transmission coefficients between 0 and 1 are presented in grayscale.

Figure 7(a) shows a 1-D transmission map for Specimen NR-E (mild damage) based on transmission coefficients measured in the vertical direction. The 1-D transmission map effectively identified the existence of surface-breaking cracks. The regions without surface-breaking cracks in visual inspection show light colors, whereas the regions with cracks show dark colors, which indicates low transmission. Overall, the 1-D transmission map based on transmission measurements in the vertical direction matched the horizontal cracks well. In addition, the darkness in the transmission map may be interpreted to show additional information about crack depths. The

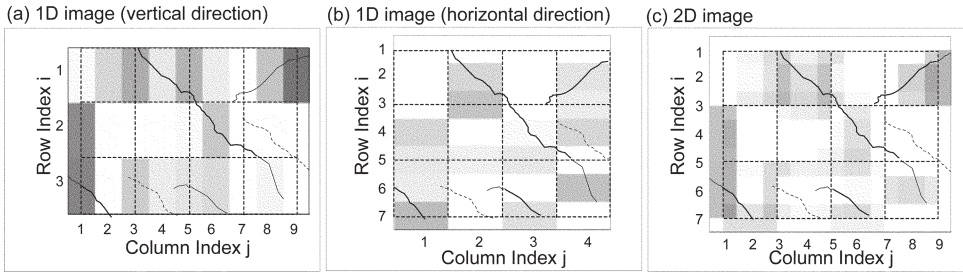

Fig. 8—Transmission maps measured from Specimen NR-W: (a) 1-D transmission map (vertical direction) with row spacing (distance between impact points) of 10 cm (3.94 in.) and column spacing (horizontal shift) of 5 cm (1.97 in.); (b) 1-D transmission map (horizontal direction) with column spacing (impact points) of 10 cm (3.94 in.) and row spacing (vertical shift) of 5 cm (1.97 in.); and (c) 2-D transmission map with combination of 1-D transmission map in vertical and horizontal directions shown in (a) and (b).

Table 1—Crack depth estimation using transmission coefficients measured by MSC and SC procedures

Specimen no.	Tr_n		h/λ	f, kHz	λ, mm (in.)	h_{ndt}, mm (in.)
R1-E	$Tr_n^4{}_{45}$	0.52	0.26	13	166 (6.54)	44 (1.75)
	$Tr_n^4{}_{46}$	0.30	0.33			54 (2.14)
	$Tr_n^4{}_{36}$	0.25	0.34			57 (2.27)
	$Tr_n^4{}_{35}$	0.42	0.29			49 (1.95)
R2-W	$Tr_n^1{}_{34}$	0.37	0.31			51 (2.02)
	$Tr_n^1{}_{35}$	0.29	0.33			54 (2.14)
	$Tr_n^1{}_{25}$	0.34	0.32			53 (2.10)
	$Tr_{n,sc}$	0.31	0.33			54* (2.14)
R2-W	$Tr_n^2{}_{25}$	0.61	0.24			40 (1.59)
	$Tr_n^4{}_{35}$	0.44	0.29			48 (1.91)
	$Tr_{n,sc}$	0.29	0.33			54* (2.14)
R2-W	$Tr_n^3{}_{23}$	0.69	0.21			34 (1.35)
	$Tr_n^3{}_{24}$	0.78	0.17			28 (1.11)
	$Tr_{n,sc}$	0.83	0.15			32* (1.27)
R2-E	$Tr_n^6{}_{57}$	0.46	0.28	15	144 (5.67)	41 (1.63)
	$Tr_n^6{}_{58}$	0.25	0.34			49 (1.95)

*Results based on transmission measurement through SC procedure.

characterization of the depths of surface-breaking cracks is discussed in detail in the next section.

The 1-D transmission maps for Specimens R1-E, R2-E, and R2-W based on the transmission coefficients measured in the vertical direction are shown in Fig. 7(b), (c), and (d). Compared to the case of Specimen NR-E, distributed surface-breaking cracks in these specimens show wider width and more complex crack patterns, which raise difficulties in transmission measurements and the interpretation of transmission maps. In Fig. 7(b), the 1-D transmission map for Specimen R1-E effectively identified the cracks; however, in Fig. 7(c) and (d) for Specimens R2-E and R2-W, some regions with observable cracks were not properly identified in the transmission maps. The possible reasons for this discrepancy may come from near-field effects and limitations of the 1-D image. Previous researchers[6,18,23] noticed that the near-field effects cause a significant enhancement in transmission measurements if the sensors are too close to a surface-breaking crack in the SC procedure. To minimize the near-field effect, the impact source spacing should not be too small.

The 1-D scan is insensitive to cracks parallel to the wave path. A two-dimensional (2-D) scan can be used to overcome the limitations of the 1-D scan.[27] Figure 8(a) and (b) shows 1-D transmission maps based on the transmission coefficients measured in the vertical and horizontal directions from Specimen NR-W (mild damage). The transmission map based on transmissions in the vertical direction matches crack patterns in the horizontal direction well, whereas the transmission in the horizontal direction matches vertical cracks. The 1-D transmission maps do not have sufficient image resolution in the measurement direction due to the limitation of specimen size and the near-field effects. However, the spatial resolution can be improved by using small spacing between scan lines. A 2-D transmission map in Fig. 8(c) was formed from the combination of Fig. 8(a) and (b). Consistent with previous findings,[27] the combined 2-D image shows better agreement with crack patterns observed on the surface of the beam. In addition, the spatial resolution of the 2-D transmission map is improved by using small scan line spacing in 1-D transmission maps.

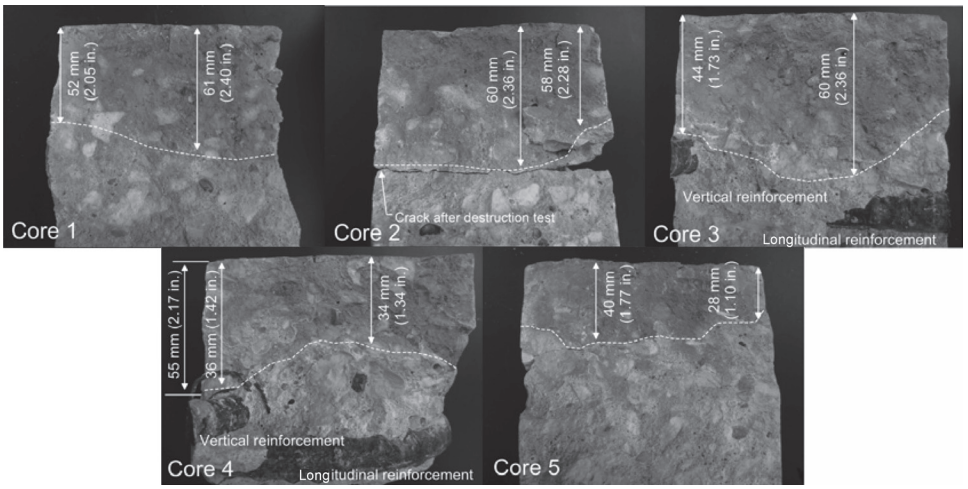

Fig. 9—Concrete core samples showing crack depths.

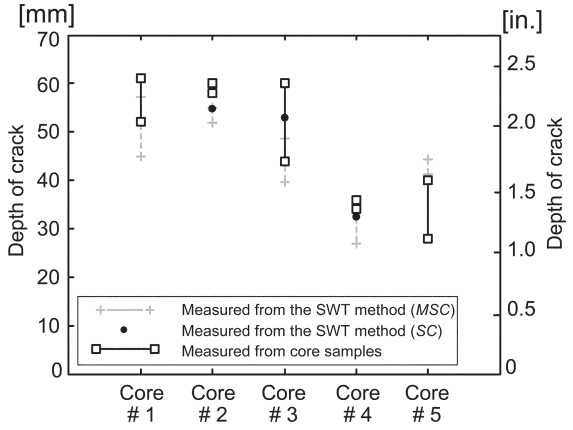

Fig. 10—Comparison of crack depths estimated using air-coupled SWT method by different sensor arrangement (MSC and SC procedures) and crack depths measured from core samples.

Crack-depth estimation using SWT method

For critical cracks identified by transmission maps and visual inspection, the depths were characterized through inversion of the transmission function in Eq. (4). In this study, the transmission coefficients were obtained in two ways: 1) the MSC procedure; and 2) the SC procedure.

In the MSC procedure, the transmission coefficients of surface waves across the critical cracks were first calculated by Eq. (5), and then depths of the cracks were estimated using the simplified SWT method at the center frequencies. Multiple impact sources can provide several sets of signal data for calculating transmission coefficients of surface waves in the region between the impact sources. The predicted depths of the critical cracks (shown in Fig. 4) are summarized in Table 1. The test regions were carefully determined to minimize the near-field effects and obtain reliable and consistent transmission functions for all the cracks. For Critical Crack 1 in Specimen R1-E (marked in Fig. 4(b)), $Tr_{n\,45}^{\,4}$, $Tr_{n\,46}^{\,4}$, $Tr_{n\,36}^{\,4}$, and $Tr_{n\,35}^{\,4}$ were used to estimate the depth of the crack. As seen in Table 1, the transmission coefficients from various regions (4-5, 4-6, 3-6, and 3-5) provided values ranging from 0.25 to 0.52, resulting in approximate crack depths ranging from 44 to 57 mm (1.73 to 2.24 in.). For other cracks, the MSC procedure provided the crack depths in ranges.

In addition, the conventional SC procedure was also applied to measure the transmission coefficients of surface waves across Critical Cracks 2, 3, and 4 (refer to Fig. 4). Transmission coefficients were calculated using Eq. (2) and (3) using the test setup presented in Fig. 1. The locations of the sensors were adjusted to leave enough space between the cracks and sensors ($x_1 = x_2 = 15$ cm [5.91 in.]). Furthermore, the impact locations were carefully chosen in solid regions. This may be effective to further minimize the near-field effects of surface waves and interaction of the surface waves between cracks. The transmission coefficients and corresponding depths of cracks are also summarized in Table 1. In three cases, the results from the SC method match the upper limit of the MSC results. The validity of the MSC and SC procedures for crack- depth estimation will be discussed in the following section.

Comparison with core samples

The SWT measurement results are compared to the direct measurements from the core samples. Five core samples were extracted from the locations of the critical cracks. Figure 9 illustrates the vertical cross sections of the core samples showing the surface of the surface-breaking cracks. The ASR crack depth is determined by measuring the darkened surface caused by dust and carbonation. Figure 9 reveals that the crack depth in concrete varies between 28 and 61 mm (1.1 to 2.4 in.). The existence of reinforcements strongly affects the extent of the cracks. The variations of crack depths are shown on the cored samples in Fig. 9.

Figure 10 compares the crack depth measured by the simplified SWT method and the core samples. The results from the SWT method show fairly good agreement with the actual crack depth measured from the core samples. Particularly, depth estimation based on the original SC procedure provides a better match with the results from the core samples. The discrepancy between the SWT results and direct measurement on the core samples may be caused by near-field effects and interaction of surface waves between multiple cracks; however, the experimental results shown in this study indicate that the SWT measurements provide valuable information in field practice.

CONCLUSIONS

In this study, the air-coupled SWT method was developed to evaluate surface-breaking cracks in in-place concrete structures. The findings obtained from this study are shown as follows:

1. Comparison analysis shows that both the air-coupled sensors and accelerometers give good signal coherence (greater than 0.98) and good agreement in a frequency range of 10 to 30 kHz, especially around the center frequency (~17 kHz). Field application in this study demonstrated that the air-coupled sensors substantially improved the test speed measurements of in-place concrete structures compared to the contact sensors.

2. The SWT method can be extended to global inspection using the MSC procedure. Using the MSC procedure, 1-D and 2-D transmission maps were obtained to identify the existence of surface-breaking cracks in concrete. The 1-D transmission map was demonstrated to be effective in identifying cracks normal to the test direction.

3. The 2-D transmission maps were obtained by a combination of the 1-D transmission maps in the horizontal and vertical directions. The combined 2-D map shows better agreement with crack patterns observed on the surface of the beam. In addition, the spatial resolution of the 2-D transmission map can be improved by using small scan line spacing in 1-D transmission maps.

4. The depths of the critical surface-breaking cracks in concrete structures were estimated by the simplified SWT method suggested in this study. Comparison analyses showed that the estimated depth from the SC and MSC procedures matched fairly well with the results measured from core samples directly extracted from the surface of the concrete beams. The results presented in this study showed that the simplified SWT procedure is a potential method to estimate the depth of a surface-breaking crack in in-place concrete structures.

ACKNOWLEDGMENTS

The beam specimens investigated in this study were moved from a construction yard to the Phil M. Ferguson Structural Engineering Laboratory at the University of Texas at Austin under a research project funded by the Texas Department of Transportation. The authors would like to gratefully acknowledge O. Bayrak and J. O. Jirsa for permission to nondestructively investigate the beam specimens.

REFERENCES

1. Lin, Y. C.; Liou, T. H.; and Tsai, W. H., "Determining Crack Depth and Measurement Errors Using Time-of-Flight Diffraction Techniques," *ACI Materials Journal*, V. 96, No. 2, Mar.-Apr. 1999, pp. 190-195.

2. Lin, Y. C., and Su, W. C., "Use of Stress Waves for Determining the Depth of Surface-Opening Cracks in Concrete Structures," *ACI Materials Journal*, V. 93, No. 5, Sept.-Oct. 1996, pp. 494-505.

3. Sansalone, M.; Lin, J. M.; and Streett, W. B., "Determining the Depth of Surface-Opening Cracks Using Impact-Generated Stress Waves and Time-of-Flight Technique," *ACI Materials Journal*, V. 95, No. 2, Mar.-Apr. 1998, pp. 168-177.

4. Krüger, M., and Grosse, C. U., "Crack Depth Determination Using Advanced Impact-Echo Techniques," *Proceedings of European Conference on NDT*, BB-103-CD, Berlin, Germany, 2006, Tu.4.2.2.

5. Song, W.-J.; Popovics, J. S.; and Achenbach, J. D., "Crack Depth Determination in Concrete Slabs Using Wave Propagation Measurements," *Proceedings for 1999 FAA (Federal Aviation Administration) Airport Technology Transfer Conference*, Atlantic City, NJ, 1999.

6. Hevin, G.; Abraham, O.; Petersen, H. A.; and Campillo, M., "Characterization of Surface Cracks with Rayleigh Waves: A Numerical Model," *NDT & E International*, V. 31, No. 4, 1998, pp. 289-298.

7. Popovics, J. S. et al., "Application of Surface Wave Transmission Measurements for Crack Depth Determination in Concrete," *ACI Materials Journal*, V. 97, No. 2, Mar.-Apr. 2000, pp. 127-135.

8. Song, W.-J.; Popovics, J. S.; Aldrin, J. C.; and Shah, S. P., "Measurement of Surface Wave Transmission Coefficient across Surface-Breaking Cracks and Notches in Concrete," *The Journal of the Acoustical Society of America*, V. 113, No. 2, 2003, pp. 717-725.

9. Achenbach, J. D.; Komsky, I. N.; Lee, Y. C.; and Angel, Y. C., "Self-Calibrating Ultrasonic Technique for Crack Depth Measurement," *Journal of Nondestructive Evaluation*, V. 11, No. 2, 1992, pp. 103-108.

10. Angel, Y. C., and Achenbach, J. D., "Reflection and Transmission of Obliquely Incident Rayleigh Waves by a Surface-Breaking Crack," *The Journal of the Acoustical Society of America*, V. 75, No. 2, 1984, pp. 313-319.

11. Hirao, M.; Fukuoka, H.; and Miura, Y., "Scattering of Rayleigh Surface-Waves by Edge Cracks: Numerical Simulation and Experiment," *The Journal of the Acoustical Society of America*, V. 72, No. 2, 1982, pp. 602-606.

12. Masserey, B., and Mazza, E., "Analysis of the Near-Field Ultrasonic Scattering at a Surface Crack," *The Journal of the Acoustical Society of America*, V. 118, No. 6, 2005, pp. 3585-3594.

13. Viktorov, I. A., *Rayleigh Waves and Lamb Waves—Physical Theory and Application*, Plenum, New York, 1967, 154 pp.

14. Yew, C. H.; Chen, K. G.; and Wang, D. L., "An Experimental Study of Interaction between Surface Waves and a Surface Breaking Crack," *The Journal of the Acoustical Society of America*, V. 75, No. 1, 1984, pp. 189-196.

15. Achenbach, J. D.; Keer, L. M.; and Mendelsohn, D. A., "Elastodynamic Analysis of an Edge Crack," *Journal of Applied Mechanics*, V. 47, No. 3, 1980, pp. 551-556.

16. Mendelsohn, D. A.; Achenbach, J. D.; and Keer, L. M., "Scattering of Elastic Waves by a Surface-Breaking Crack," *Wave Motion*, V. 2, No. 3, 1980, pp. 277-292.

17. Cheng, A., and Achenbach, J. D., "A Roller Device to Scan for Surface-Breaking Cracks and to Determine Crack Depth by a Self-Calibrating Ultrasonic Technique," *Research in Nondestructive Evaluation*, V. 7, No. 4, 1996, pp. 185-194.

18. Kee, S. H., and Zhu, J., "Using Air-Coupled Sensors to Determine the Depth of a Surface-Breaking Crack in Concrete," *The Journal of the Acoustical Society of America*, V. 127, No. 3, Mar. 2010, pp. 1279-1287.

19. Shin, S. W.; Zhu, J.; Min, J.; and Popovics, J. S., "Crack Depth Estimation in Concrete Using Energy Transmission of Surface Waves," *ACI Materials Journal*, V. 105, No. 5, Sept.-Oct. 2008, pp. 510-516.

20. Blackshire, J. L., and Sathish, S., "Near-Field Ultrasonic Scattering from Surface-Breaking Cracks," *Applied Physics Letters*, V. 80, No. 18, 2002, pp. 3442-3444.

21. Edwards, R. S.; Jian, X.; Fan, Y.; and Dixon, S., "Signal Enhancement of the In-Plane and Out-of Plane Rayleigh Wave Components," *Applied Physics Letters*, V. 87, No. 19, 2005, pp. 194,104 to 194,104-3.

22. Jian, X.; Dixon, S.; Guo, N.; and Edwards, R., "Rayleigh Wave Interaction with Surface-Breaking Cracks," *Journal of Applied Physics*, V. 101, 2007, pp. 064,906 to 064,906-7.

23. Kee, S.-H., and Zhu, J., "Effects of Sensor Locations on Air-Coupled Surface Wave Transmission Measurements," *IEEE Transaction on Ultrasonics, Ferroelectrics and Frequency*, V. 58, No. 2, 2011, pp. 427-436.

24. Kee, S.-H., and Zhu, J., "Surface Wave Transmission Measurement across Distributed Surface-Breaking Cracks Using Air-Coupled Sensors," *Journal of Sound and Vibration*, V. 330, No. 22, 2011, pp. 5333-5344.

25. Wang, T.-W., "Shear Performance of ASR/DEF Damaged Prestressed Concrete Trapezoidal Box Bridge Girders," PhD dissertation, The University of Texas at Austin, Austin, TX, 2010, 345 pp.

26. Zhu, J., "Non-Contact NDT of Concrete Structures Using Air-Coupled Sensors," PhD dissertation, University of Illinois at Urbana-Champaign, Urbana, IL, 2005, 105 pp.

27. Zhu, J., and Popovics, J. S., "Non-Contact Imaging for Surface-Opening Cracks in Concrete with Air-Coupled Sensors," *Materials and Structures*, V. 38, 2005, pp. 801-806.

28. Zhu, J., and Popovics, J. S., "Imaging Concrete Structures Using Air-Coupled Impact-Echo," *Journal of Engineering Mechanics*, ASCE, V. 133, No. 6, June 2007, pp. 628-640.

29. Zhu, J.; Popovics, J. S.; and Schubert, F., "Leaky Rayleigh and Scholte Waves at the Fluid-Solid Interface Subjected to Transient Point Loading," *The Journal of the Acoustical Society of America*, V. 116, No. 4, Oct. 2004, pp. 2101-2110.

30. Eisner, L., and Clayton, R. W., "A Reciprocity Method for Multiple-Source Simulations," *Bulletin of the Seismological Society of America*, V. 91, No. 3, 2001, pp. 553-560.